Supplementary Information

Fabrication of Low-dimensional Network Polymers with Thermoresponsive Properties Using MOF Scaffolds

Yuki Kametani, †[a] Ami Nishijima, †[b] Shu Hiramoto [c] and Takashi Uemura *[a,b]

† These authors contributed equally to this article.

[a] Institute of Engineering Innovation, School of Engineering, The University of Tokyo, 7-3-1 Hongo, Bunkyo-ku, Tokyo 113-8656, Japan.
[b] Department of Applied Chemistry, Graduate School of Engineering, The University of Tokyo, 7-3-1 Hongo, Bunkyo-ku, Tokyo 113-8656, Japan.
[c] Department of Advanced Materials Science, Graduate School of Frontier Sciences, The University of Tokyo, 7-3-1 Hongo, Bunkyo-ku, Tokyo 113-8656, Japan

*uemurat@g.ecc.u-tokyo.ac.jp

Contents

1. General

^{1}H nuclear magnetic resonance (NMR) spectra were recorded using Bruker Avance III HD (500 MHz) spectrometers equipped with a PABBO probe. X-ray powder diffraction (XRPD) data were recorded using a Rigaku SmartLab X-ray diffractometer with Cu Kα radiation.

Gel permeation chromatography (GPC) was performed at 60 °C on a SHIMADZU model LC-2050 system equipped with two polystyrene gel columns in series (Shodex KD-806M and KD-802) and refractive index and UV detectors. The mobile phase was *N*,*N*-dimethyl formamide (DMF) containing 10 mM LiBr at a flow rate of 1.0 mL/min. The number-average molecular weight (M_n) and molecular weight distribution (M_w/M_n) were determined relative to a polystyrene standard (SM-105, Shodex).

Scanning electron microscopy (SEM) was performed using a Hitachi High-Tech Science Corporation model SU5000 instrument. The samples were deposited on a conducting carbon tape attached to an SEM sample holder and coated with osmium.

Atomic force microscopy (AFM) was performed by noncontact tapping mode using an Oxford Instruments MFP-3D Origin instrument (Asylum Research AFM). Aluminum-coated cantilevers (OMCL-AC240TS-R3, Olympus) with spring constants of 0.6–3.5 pN/nm (resonant frequency: 70 kHz) were used, which were calibrated by the thermal fluctuation method. The Igor Pro software (WaveMetrics) was used for data acquisition and analysis. For the observation of single polymer objects (Figure 3 and Figure S5), the AFM samples were prepared by dissolving PNIPAm samples in $CHCl_3$ and spin-casting (2000 rpm, 5 sec) onto a mica substrate. The concentration of spin-casted solutions was as follows, **PNIPAm-1D** = 2 mg/L, **PNIPAm-2D** = 150 mg/L, and **PNIPAm-3D** = 1 g/L. To obtain a clear image for **PNIPAm-1D**, a high molecular weight fraction of the polymer (M_n = 192,000, M_w/M_n = 1.31, polystyrene standard) was collected by preparative GPC. For the observation of particle assemblies of **PNIPAm-1D** and **PNIPAm-2D** (Figure S12), the aqueous dispersions (1 g/L) were spin-casted (2000 rpm, 60 sec) onto a mica substrate.

Transmittance of the polymers solution was measured on a V-670 spectrophotometer (Jasco, optical path length = 1.0 cm, λ = 670 nm, heating rate = 10 ˚C/h or 2 ˚C/h). The polymer samples for transmittance measurement were dissolved in deionized water (1 g/L), stored in a refrigerator (~4 ˚C) for more than one day, and then filtered using a 5 μm syringe filter before the measurement.

Dynamic light scattering (DLS) measurements were performed for aqueous PNIPAm solutions (1 g/L) on a Malvern Zetasizer equipped with a He-Ne laser (λ= 633 nm). The light-scattering signal was detected at a fixed angle of 173°. The hydrodynamic diameter (D_h) was determined from the peak value of the volume-weighted size distribution.

Molecular dynamics (MD) simulation was performed using the Materials Studio v4.4 software package (Accelrys Inc.) with the Universal Force Field, as implemented in the Forcite module. Charges were accounted for using the charge equilibration method. The initial structure of **1** was generated based on its crystal structure. After geometrical optimization, the dynamics were conducted at 493 K for 50 ps under NVT conditions.

2. Materials

All reagents and chemicals were obtained from commercial sources unless otherwise noted. *N*-isopropylacrylamide (NIPAm; TCI, >99.8%) was recrystallized from toluene / hexane (*v*/*v* = 1 : 1). Ethylene glycol dimethacrylate (EDMA; Wako, >97%) was passed through an inhibitor remover column (Aldrich) before use. Host MOFs, $[In(OH)bdc]_n$ (**1**, bdc: 1,4-benzenedicarboxylate)[1] and $[Ni(Hbtc)(dpb)]_n$ (**2**, btc: 1,3,5-benzenetricarboxylate, dpb: 1,4-di(pyridin-4-yl)benzene)[2,3] were synthesized according to the literature.

3. Supplementary Figures

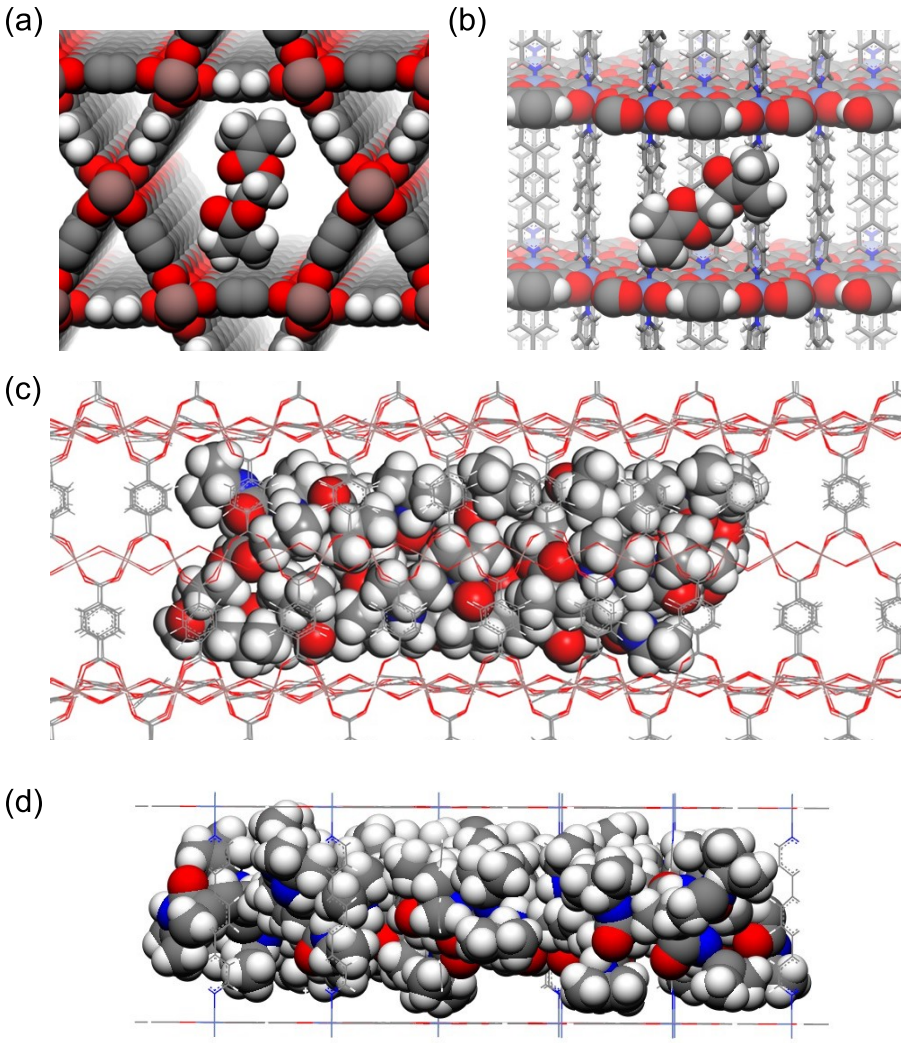

Figure S1. Molecular models of EDMA crosslinker introduced into (a) **1** and (b) **2**. MD structures of (c) **PNIPAm-1D** accommodated in a nanochannel of **1** and (d) **PNIPAm-2D** confined between the interstice of **2**. Atoms: In (brown), Ni (purple), O (red), N (Blue), C (gray), H (white). For clarity, the pillar ligands (dpb) in (b) are shown as stick models, and MOFs in (c) and (d) are depicted as line models.

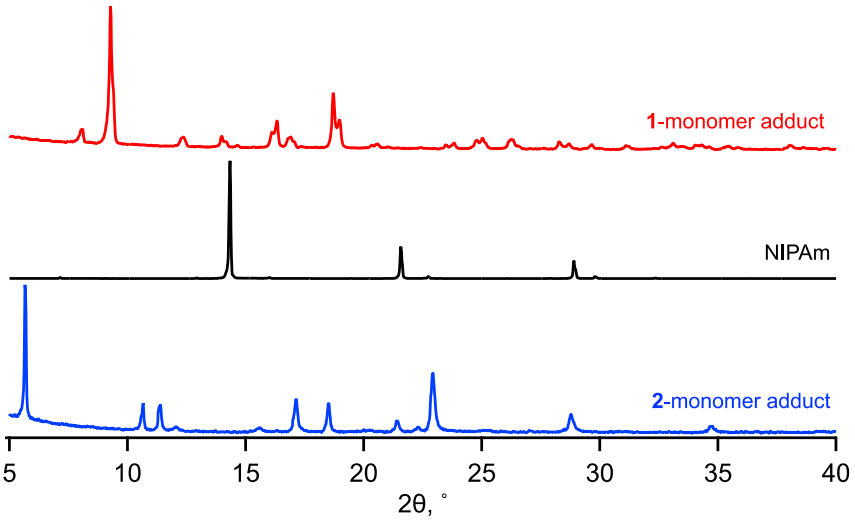

Figure S2. XRPD patterns of **1**-monomer adduct (red), neat NIPAm (black), and **2**-monomer adduct (blue). Peaks for the neat NIPAm were not detectable in the patterns of the MOF-monomer adducts, showing the introduction of the monomer only inside the pores.

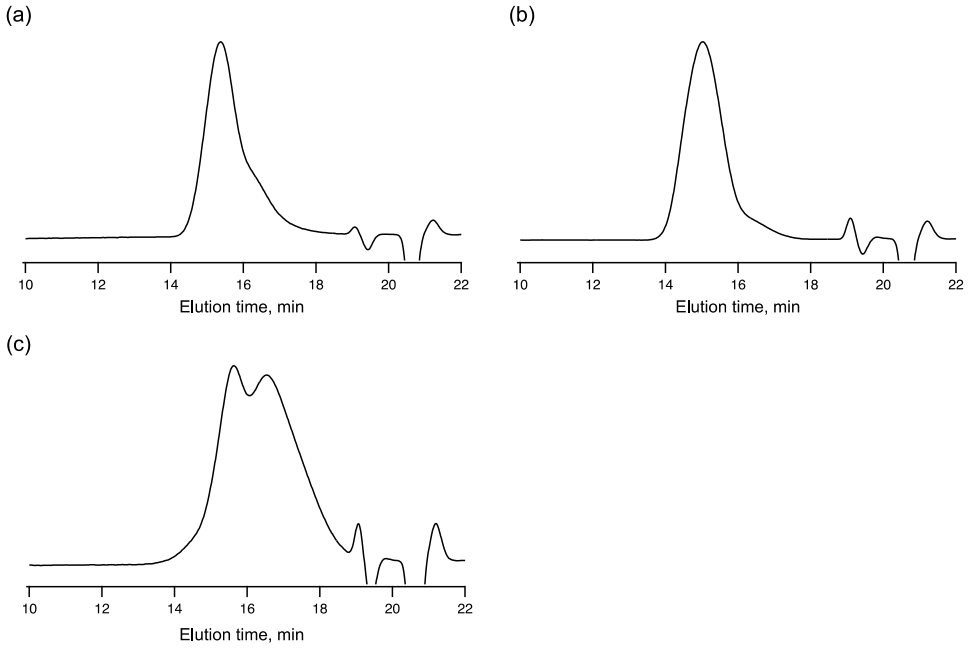

Figure S3. GPC curves of (a) **PNIPAm-L**, (b) **PNIPAm-1D**, and (c) **PNIPAm-2D**. GPC measurement of **PNIPAm-3D** was not carried out because the particle size was too large.

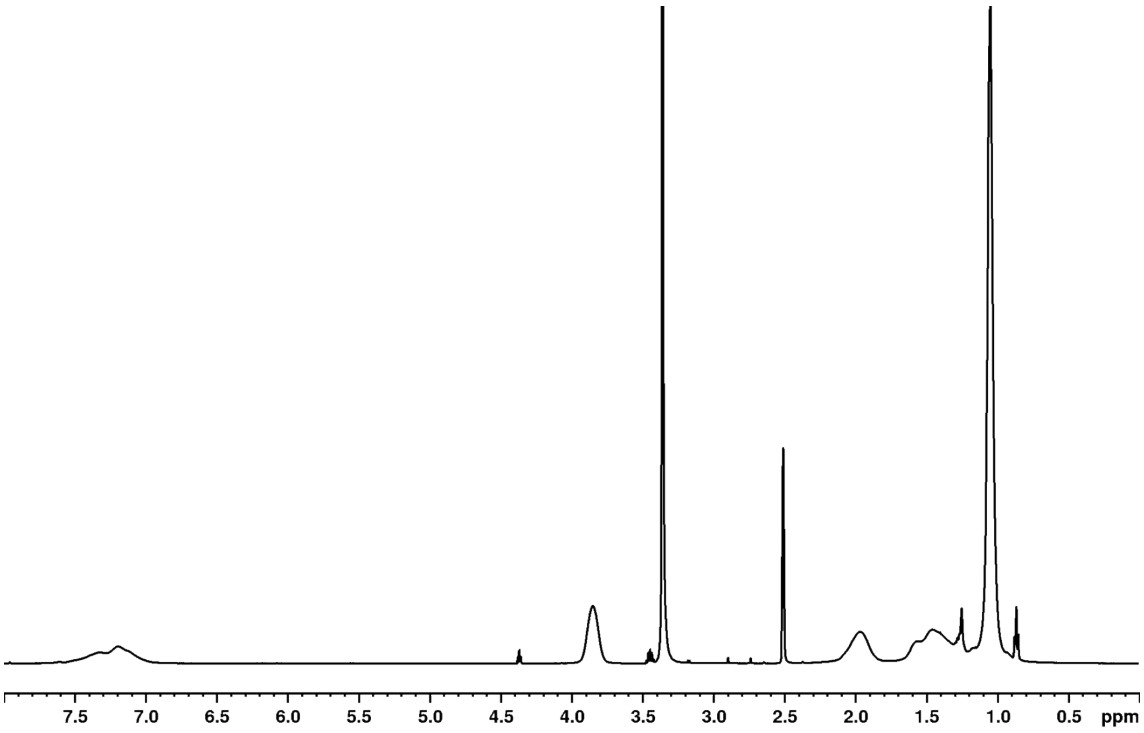

Figure S4. ^{1}H NMR spectrum of **PNIPAm-L** in DMSO-d_6.

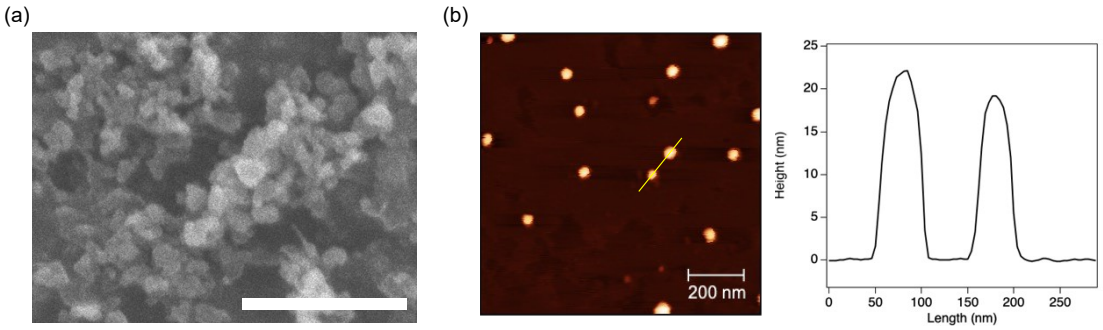

Figure S5. (a) SEM image of **PNIPAm-3D** (scale bar 1 μm). (b) AFM image and height profile of **PNIPAm-3D**. Samples were deposited on a mica substrate by spin-casting dilute $CHCl_3$ solutions thereof. The height profile was recorded along the yellow line in the image. The size of the observed spherical nanoparticles roughly agreed with that determined from DLS measurement (Figure 5).

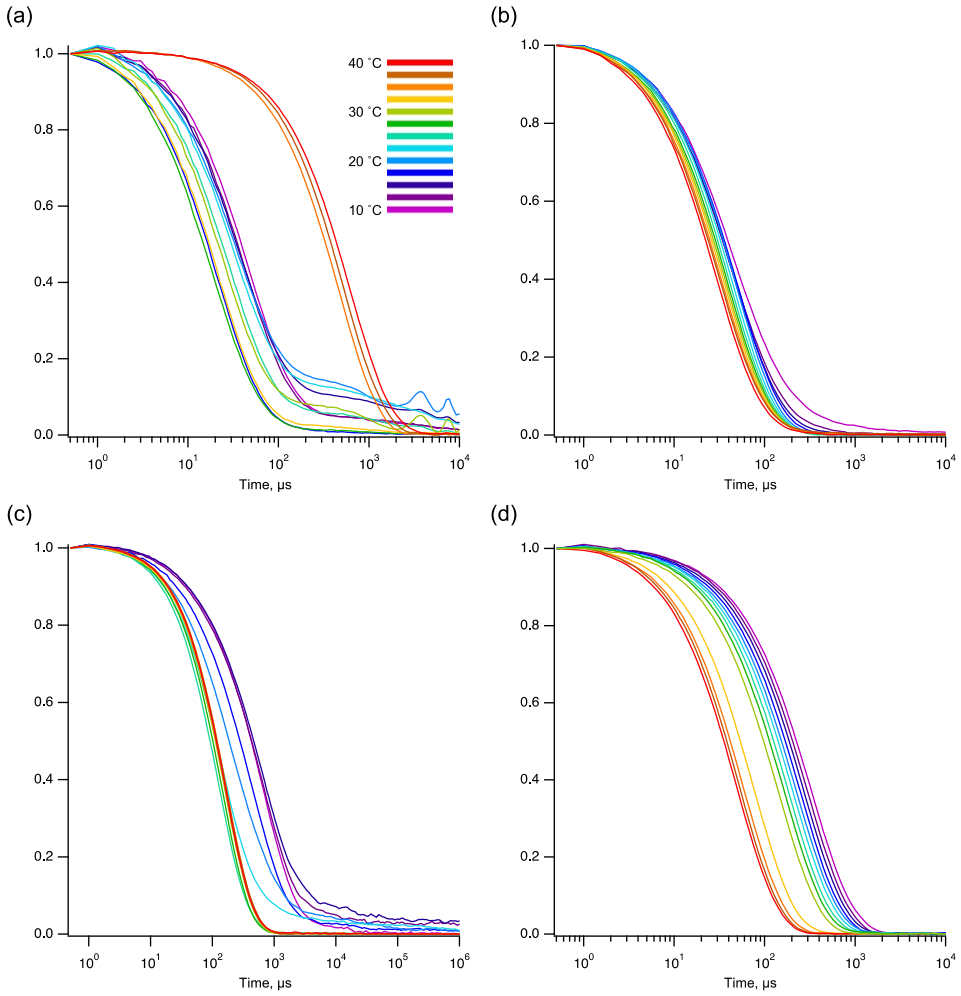

Figure S6. Normalized autocorrelation function of (a) **PNIPAm-L**, (b) **PNIPAm-1D**, (c) **PNIPAm-2D**, and (d) **PNIPAm-3D** in water at different temperatures. For **PNIPAm-L**, the calculation of D_h was not performed due to multiple scattering caused by high turbidity. However, the significant shift observed in the autocorrelation function suggests that the particle size dramatically increased before and after the phase transition.

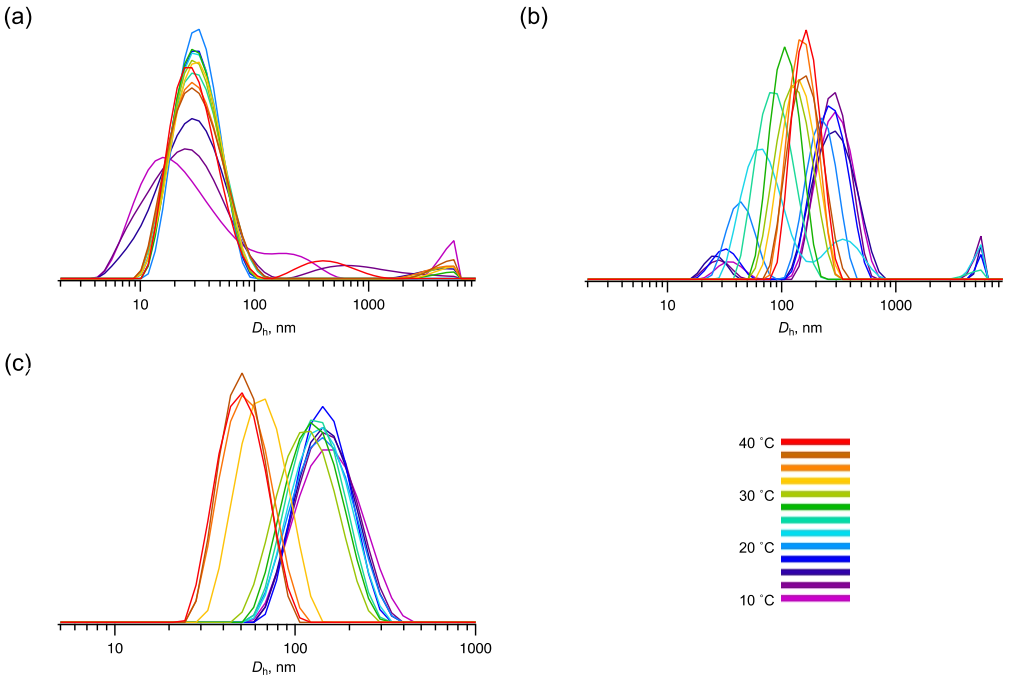

Figure S7. Intensity-weighted size distributions of (a) **PNIPAm-1D**, (b) **PNIPAm-2D**, and (c) **PNIPAm-3D** in water at different temperatures. Since the scattering intensity scales with the sixth power of particle diameter, the population of large particles are overestimated in this distribution.

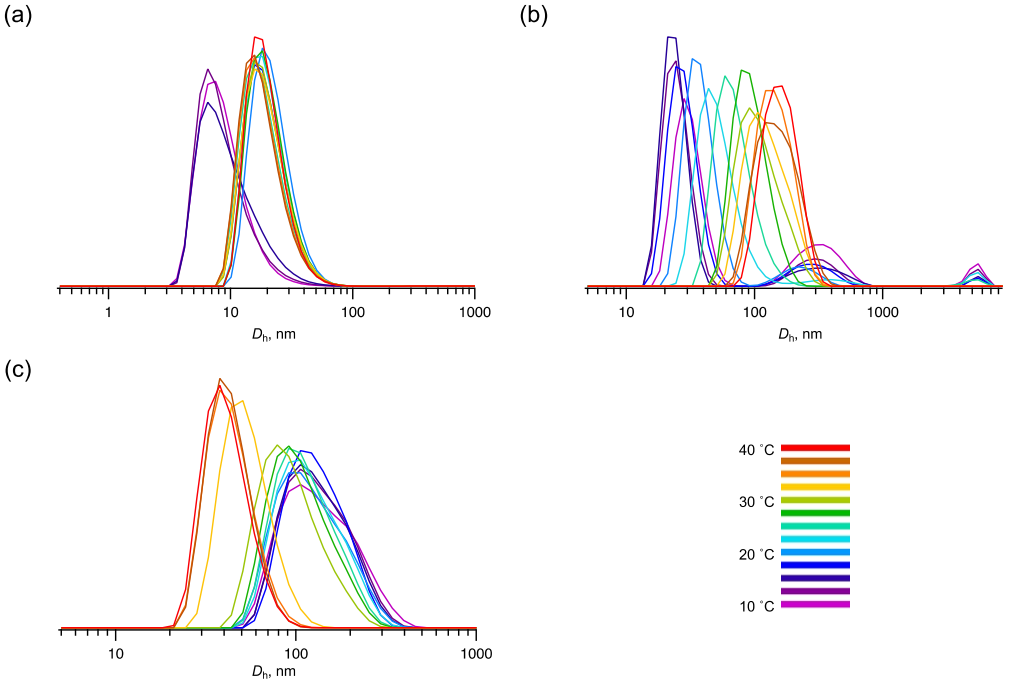

Figure S8. Volume-weighted size distributions of (a) **PNIPAm-1D**, (b) **PNIPAm-2D**, and (c) **PNIPAm-3D** in water at different temperatures.

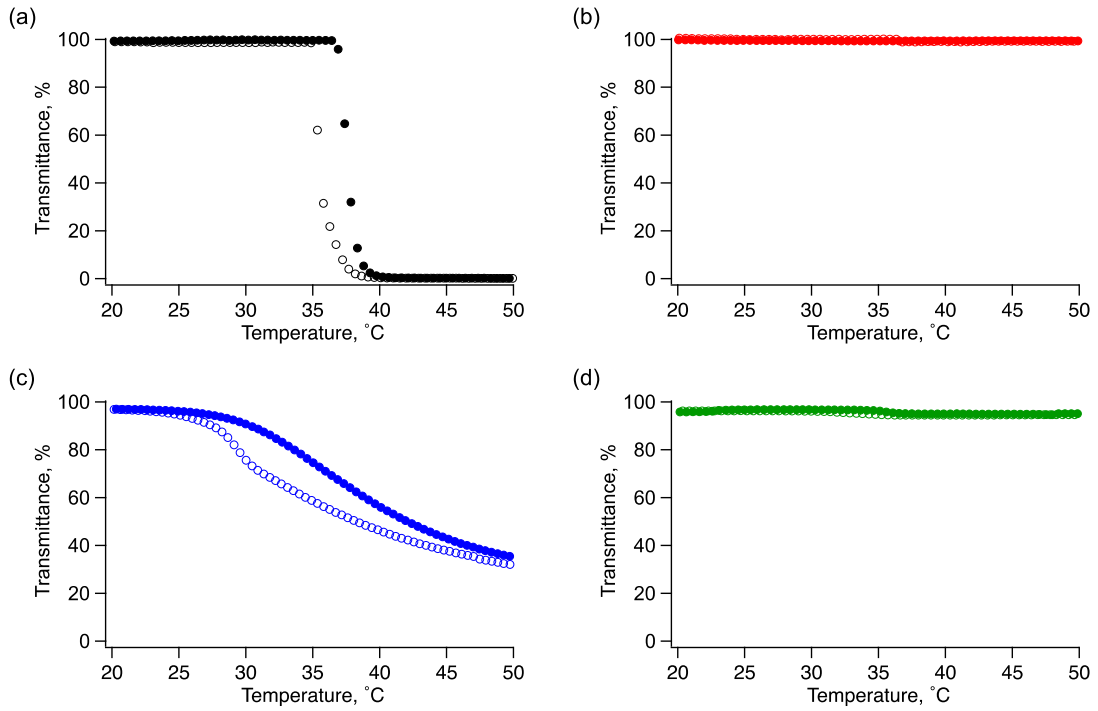

Figure S9. Temperature dependences of optical transmittance for aqueous solutions of (a) **PNIPAm-L**, (b) **PNIPAm-1D**, (c) **PNIPAm-2D**, and (d) **PNIPAm-3D**, plotted for heating (filled) and cooling (open) processes. The heating and cooling rates were 10 ˚C/h.

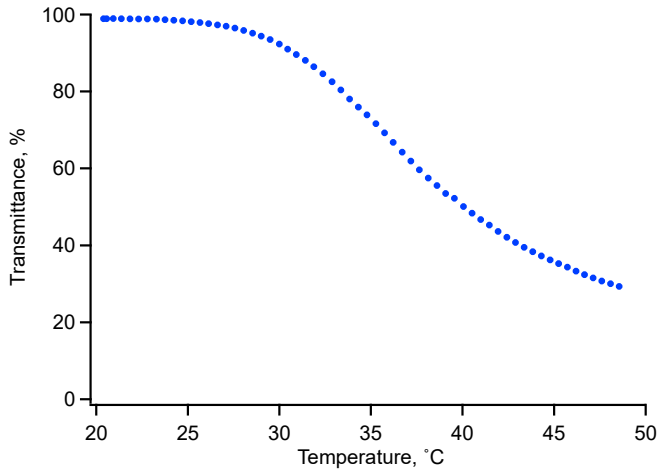

Figure S10. Temperature dependences of optical transmittance for aqueous solutions of **PNIPAm-2D** with the heating rate of 2 ˚C/h.

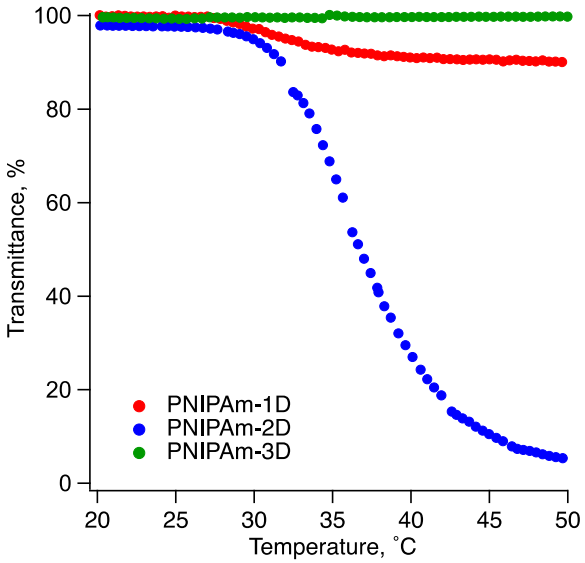

Figure S11. Temperature dependences of optical transmittance for aqueous solutions of **PNIPAm-1D** (red), **PNIPAm-2D** (blue), and **PNIPAm-3D** (green) with the cross-linking ratios of 4 mol%, 3 mol%, and 4 mol%, respectively. The heating and cooling rates were 10 ˚C/h.

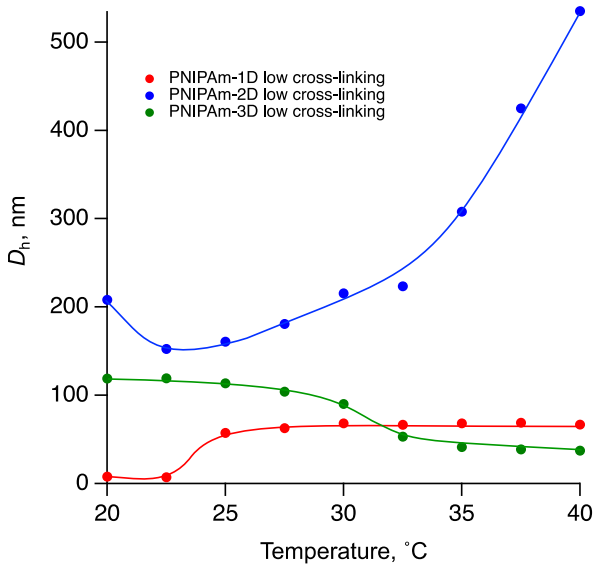

Figure S12. Temperature dependences of hydrodynamic diameters of **PNIPAm-1D** (red) and **PNIPAm-2D** (blue), and **PNIPAm-3D** (green) with the cross-linking ratio of 4 mol%, 3 mol%, and 4 mol%, respectively. Transition temperatures of these samples were slightly higher than those of the corresponding polymers with higher cross-linking ratios (Figure 5).

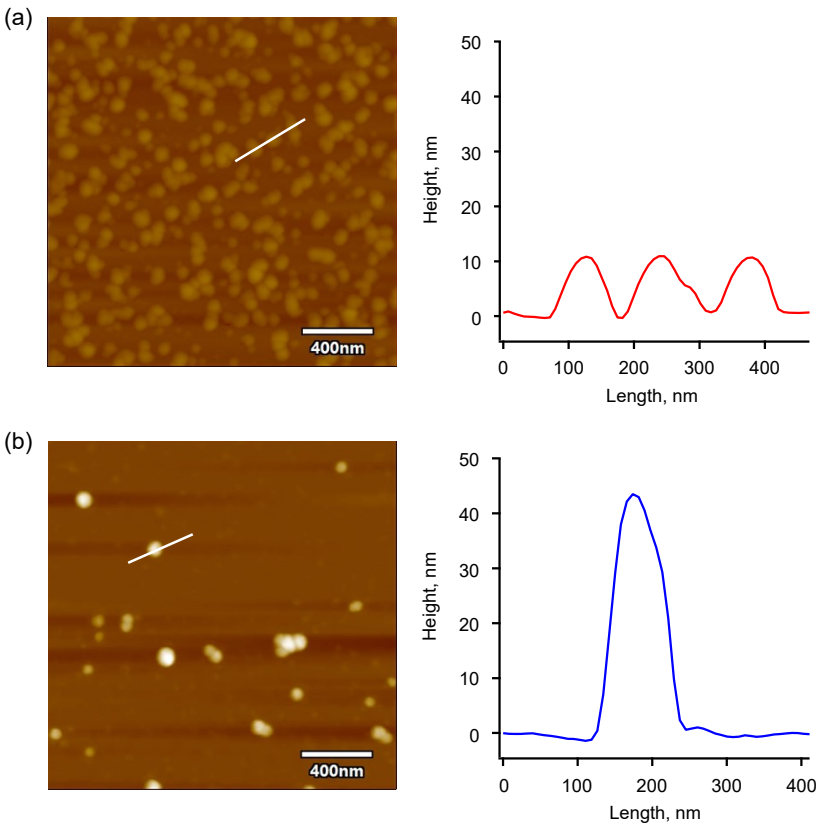

Figure S13. AFM images of **PNIPAm-1D** and **PNIPAm-2D** deposited on a mica substrate from aqueous solutions (1 g/L) at room temperature (~28 °C), which is above the onset temperature of the transition.

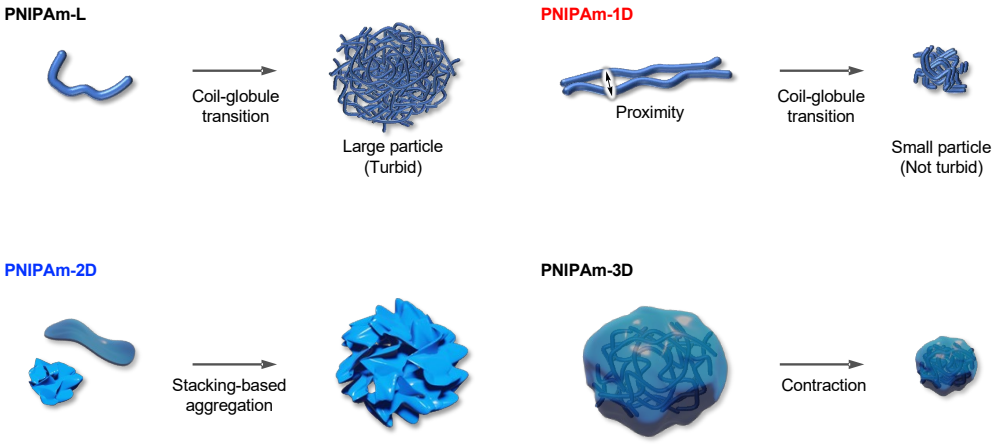

Figure S14. Schematic image of plausible thermoresponsive behaviors that PNIPAm showed in this work.

4. Supplementary References

(1) C. Volkringer, M. Meddouri, T. Loiseau, N. Guillou, J. Marrot, G. Férey, M. Haouas, F. Taulelle, N. Audebrand, M. Latroche, *Inorg. Chem.*, 2008, **47**, 11892.

(2) C. Gao, S. Liu, L. Xie, Y. Ren, J. Cao, C. Sun, *CrystEngComm.*, 2007, **9**, 545.

(3) N. Hosono, S. Mochizuki, Y. Hayashi, T. Uemura, *Nat. Commun.*, 2020, **11**, 3573.